Microstructures and Surface Stabilities of Ni-0.4C-6Ta-xCr, $0 \leq x \leq 50$ Wt Pct Cast Alloys at High Temperature

Patrice Berthod

Microstructure and surface stabilities of {Ni-0.4C-6Ta-xCr, $0 \leq x \leq 50$ wt.%} cast alloys at high temperature

Patrice Berthod[1,2]

[1]*Faculty of Science and Technologies*
[2]*CNRS, Institut Jean Lamour (UMR 7198), Department CP2S*
[1,2]*University of Lorraine, Postal Box 70239, 54506 Vandoeuvre-lès-Nancy, FRANCE*

patrice.berthod@centraliens-lille.org

Postprint of the article **METALLURGICAL AND MATERIALS TRANSACTIONS A, VOLUME 49A,**

JUNE 2018, 2311—2323; https://doi.org/10.1007/s11661-018-4574-7

Abstract. Nickel-based cast alloys rich in chromium and reinforced by TaC carbides are potentially very interesting alloys for applications at elevated temperatures. Unfortunately, unlike cobalt-chromium and iron-chromium alloys, it is difficult to obtain exclusively TaC as primary carbides in Ni-Cr alloys. In alloys containing 30 wt.% Cr tantalum, carbides coexist with chromium carbides. The latter tend to weaken the alloy at elevated temperatures because they become rapidly spherical and then quickly lose their reinforcing effect. In this work, we attempted to stabilize TaC as a single carbide phase by testing different chromium contents in the [0; 50 wt.%] range. Six alloys containing 0.4C and 6Ta, weight contents corresponding to equivalent molar contents, were elaborated by foundry, and their as-cast microstructures were characterized. Samples of all alloys were exposed to 1127°C and 1237°C for 24 hours to characterize their stabilized microstructures. The surface fractions of chromium carbides and tantalum carbides were measured by image analysis, and their evolutions versus the chromium content were studied. For the chosen C and Ta contents, it appears that obtaining TaC only is possible by decreasing the chromium content to 10 wt.%. At the same time, TaC fractions are unfortunately too low because a large portion of tantalum integrates into the solid solution in the matrix. A second consequence is a critical decrease in oxidation resistance. Other possible methods to stabilize TaC as a single carbide are evocated, such as the simultaneous increase in Ta and decrease in chromium from 30 wt.% Cr.

Keywords: Cast nickel-based alloys; High tantalum content; Varying chromium content; As-cast microstructures; High temperature microstructures; Hardness; High temperature oxidation

INTRODUCTION

Polycrystalline refractory alloys based on nickel, containing high chromium content and strengthened by carbides were among the first superalloys to be used for applications at high temperatures involving severe mechanical and chemical conditions. Currently, chromium-rich Co or Ni-based alloys elaborated by classical foundry and efficiently reinforced by eutectic MC-carbides appear to be very interesting superalloys for use at temperatures close to 1200°C. They merit efforts for further development, although current studies are still predominantly focused on Ni-based alloys - and recently also on Co-based alloys - preferentially containing Al rather than Cr.

Indeed, most of the widely used modern nickel-based superalloys contain elevated concentrations of aluminum. This is notably the case for gamma/gamma prime (γ/γ') ones belonging to the single-crystal family [1]. Their superior creep strength at high temperature is due to optimized γ' - precipitation achieved by multi-stage heat-treatments adapted for each chemical composition [2]. Their oxidation resistance is attributed to the presence of Al and Cr, as well as to other minor elements. Owing to its easy oxidation (very low Gibbs energy of formation of alumina Al_2O_3 [3]), aluminum spontaneously forms and develops as an external layer made of alumina, which is particularly efficient in protecting the subjacent alloy [4]. Unfortunately, when the usage temperature is too high (> 1100°C), the γ' precipitates tend to disappear. In addition, when the superalloy is in contact with some liquid or condensed substances (e.g., molten glass), alumina possibly dissolves in the melt. In such cases, other methods must be found to mechanically strengthen the alloys at very high temperatures and to prevent too rapid hot corrosion. Some previous solutions can be reconsidered, such as the reinforcement by carbides and the introduction of more chromium into the chemical composition. When the carbide-forming metal and the Cr content are judiciously chosen, enhanced resistance to significant stresses and to multiple aggressive environments may be obtained. The polycrystalline superalloys exploiting these well-known trends currently perform as modern superalloys at temperatures lower than 1150°C. Additionally, they may behave correctly under stresses at temperatures higher than the γ' solvus ones, as well as in the case of long-term contact with corrosive molten substances [5,6].

Chromium carbides were among the very first carbides to be used to strengthen refractory alloys [7], and later, other carbides appeared, such as the MC-type family and notably the tantalum monocarbide TaC [8]. In addition to some Ta-based [9] or heavily Ta-alloyed very refractory alloys [10], recently published works have demonstrated

that tantalum may be currently encountered in many high-temperature alloys. One can find it in numerous high entropy alloys (HEAs), in which it can be mixed with (Ti, Zr, V, Mo) [11], (Mo, Nb, Zr, Ti) [12], (Nb, Mo, W) [13, 14], (Hf, Ti, Nb, Zr) [15, 16] or (Co, Cr, Fe, Ni) [17], for instance. Other types of alloys currently developed for high temperature applications also include significant contents of Ta, such as the γ'-reinforced Co-Al-W alloys [18, 19] and Co-Re alloys [20]. However, tantalum is also frequently found to be combined with carbon in alloys devoted to uses at very high temperatures. The TaC carbide, which has been used for more than fifty years (e.g., exploited in cermets [21]), plays a strengthening role in some rather old cobalt-based alloys. A first example is the one named Mar-M509 [22], which has existed for many years now. Other examples are the conventional but rather recent cobalt-based alloys [23-26] devoted to constituting the hottest working parts in glass industry processes. TaC introduction into the microstructures of cast Fe-based alloys [27] and Ni-based alloys [28-32] was also recently attempted. Among the Co-based, Fe-based and Ni-based alloys containing Cr and TaC, the nickel alloys probably represent the family of alloys that offers the highest potential for properties at high temperatures of service. Indeed, with generally much better oxidation and corrosion resistances at high temperature than cobalt-based alloys (easier volume diffusion of Cr) and much higher intrinsic strength than iron-based alloys (austenitic, rather than ferritic, matrix), cast chromium-rich nickel alloys represent the best base for developing high performance alloys exploiting TaC carbides. Unfortunately, recent works (e.g., [28, 30, 31]) have shown that these carbides are not very stable in nickel-based alloys, notably in the presence of significant quantities of chromium, even when Ta and C are added with high contents. For example, in Ni-30 wt.% Cr alloys, the presence of 0.4 wt.% C and 6 wt.% Ta, i.e., weight contents corresponding to a molar equivalence between Ta and C, only limited quantities of TaC can be obtained after solidification and cooling. At the same time, a significant fraction of chromium carbides is also present in these alloys. Furthermore, during high temperature exposures, the TaC carbides fragment and coalesce. These phenomena are slower than those for chromium carbides, but the TaC fragmentation and coalescence are nevertheless too rapid to allow profiting from the TaC strengthening during long enough durations [28].

Nevertheless, it may be possible to develop superalloys that push the service temperature limits beyond 1150°C by taking advantage of the high chemical resistance of a Ni-Cr base and the efficient strengthening by TaC carbides. However, solutions must be found to improve the sustainability of the reinforcing TaC carbide network, which is threatened by chromium because of its tendency to act as a competitor for tantalum in the formation of carbides. To

obstruct this deleterious effect of Cr, it is important to better understand the influence of the chromium content in alloys on the stability of TaC. This is the purpose of the present work. Here, a rather wide range of Cr weight contents will be explored, from 0 to 50%, to experimentally investigate the microstructure variation of Ni-xCr-0.4C-6Ta (wt.%) with the choice of a given Cr content at solidification as well as during high temperature stages. A series of alloys will be elaborated by classical foundry in an inert atmosphere. Their microstructures at the end of post-solidification cooling, as well as after isothermal exposure at two levels of high temperature, will be characterized. Because Cr plays an important role in the resistance of alloys against hot oxidation, the surface states of the alloys aged at high temperature will be observed to determine the possible consequences for the oxidation behavior of the alloys due to changes in Cr content made to optimize the carbide population.

EXPERIMENTAL

Choice and synthesis of the alloys for the study

The Ni(bal.)-30Cr-0.4C-6Ta composition, the subject of earlier works, was taken here as the base of the series of alloys for elaboration. On one side, the Cr content was decreased in slices of 10 wt.% (20, 10 and 0 wt.% Cr in the alloy) and increased in the same way (40 and 50 wt.% in the alloy). For each chosen composition, preliminary estimation of the liquidus temperature was carried out by performing thermodynamic calculations using Thermo-Calc software (version N) to anticipate any difficulty in melting because of a too high liquidus temperature for some of the alloys. The obtained theoretical value of the liquidus temperature continuously decreases from 1420°C for 0 wt.% Cr down to 1306°C for 50 wt.% Cr. This shows that no problem may be expected for the furnace that will be used. The charges to melt were prepared. For this, a mixture of pure elements (>99.9 purity, Alfa Aesar) was constituted by weighing small portions using a precision balance. The obtained charge was placed in the fusion chamber of a furnace. Prior to heating and melting, an internal inert atmosphere was obtained by replacing air with 300 millibars of pure Ar. The high frequency induction furnace (CELES, France) was used as follows: input voltage increased from 0 to 5000 Volts, frequency rated at approximately 110 kHz, constant heating during three minutes after apparent complete melting, and decrease in input voltage to allow liquid state cooling, solidification and solid state cooling. The previously described thermal cycle was applied a second time to allow total melting of the pure

elements initially introduced and to favor good chemical homogenization of the liquid alloy. After total cooling, an ingot weighing approximately 40 grams was obtained to carry out the following characterizations and tests.

High temperature exposure tests

Each obtained ingot was divided into four parts by cutting (Buehler Delta Abrasimet metallographic saw). One of them was kept as the as-cast microstructure control, two were prepared for exposure to high temperature, and the last one was kept in reserve. The two parts destined for high temperature exposures were ground all around using 1200-grit SiC paper and placed in a resistive furnace (Nabertherm) to be exposed at a T1 temperature of 1150°C for one of them and at a T2 temperature approximately 100°C higher for the second one. Thus, six samples coming from the six ingots were simultaneously exposed for 24 hours to T1 during the same run. Similarly, six samples from the same ingots were exposed together to T2 for 24 hours. A thermocouple placed very close to the six samples allowed measuring the stabilized temperatures really obtained: these temperatures appeared to be 1127°C in the case of T1 and 1237°C for T2. These temperatures remained constant throughout the exposure. These values, 1127°C and 1237°C, which were slightly lower than the target temperatures (1150 and 1250°C), were considered to be the real temperatures of the applied isothermal exposures.

Preparation of the metallographic samples

For each alloy, metallographic samples were prepared from the as-cast part and from the two aged parts. In the case of the aged parts, two types of investigations were performed: the characterization of not only the aged microstructures but also the external and subsurface oxidation states. This is why, before embedding and polishing, the aged samples were carefully handled, and they benefited from the specific preparation: they were coated by a thin layer of gold by cathodic pulverization to allow the subsequent electrolytic deposition of a protective nickel shell all around. After approximately two hours of cathodic polarization under 0.016 A/cm² in a 50°C-maintained Watt's bath, the samples were ready to be cut with minimal risk of loss of the external oxide scales. Cutting into two halves was carried out with the same metallographic saw as previously used for separating the ingots into the initial four parts.

The as-cast parts and the halves of the oxidized samples were then embedded in a cold resin mixture, ground and polished. Grinding was achieved using SiC papers (240-grit to 1200-grit). This was followed by intermediate washing to remove any undesirable hard particles. Samples were finally finished with textile enriched with 1 µm alumina or diamond paste.

Microstructure and cross-sectional surface state characterization

The obtained mirror-like-state samples were examined using a scanning electrons microscope (SEM) of the JEOL JSM-6010-LA type, back-scattered electron (BSE) imaging and energy dispersive spectrometry (EDS) analysis. The obtained chemical compositions were assessed by EDS full frame analysis of the sample centers. The bulk microstructures of the six alloys in their as-cast state and in their two aged states were characterized by phase identification (BSE images and EDS spot analyses) and phase surface fraction (image analysis of SEM/BSE micrographs). Additionally, X-ray diffraction (XRD) was carried out on the as-cast NCT5 alloy using a Philips X'Pert Pro diffractometer to complete the identification of the phases present in this alloy particularly rich in chromium. This was the single use of XRD since this technique was not applicable to identifying the phases other than matrix because of the too small surface fractions of these minor phases (e.g., carbides). The chemical composition of the matrix was notably measured for all alloys in all their states. The surface and subsurface changes due to high temperature oxidation were also observed with the SEM in BSE mode. The different oxides present externally or internally, as well as the Cr content in the extreme surface (in the alloy but very close to the interface separating the alloy and the external oxide scale), were specified by EDS spot analysis. The depth of disappearance of the initial carbides, or other phase, from the alloy/oxide scale interface was measured. The thickness of the external oxides was not systematically determined because of the loss of the scales in many cases due to severe oxide spallation during cooling.

The quantification of the oxidation products only concerned the internal oxides, which formed a very irregular subsurface sequence of pale oxides close to the oxidation front. Image analysis was used considering not only the pale oxides present in the subsurface (major part) but also the ones mixed with the external scale (minor part) to specify an equivalent thickness according to the following steps:

- orientating the width of the rectangular imaging window parallel to the oxidation front;

- rating the detection gray level to only consider the pale internal oxides (oxides of tantalum/chromium), determining the number of white pixels with regard to the total number of pixels in the image, and calculating the surface fraction;
- multiplying by the whole real surface (e.g., 10,837 µm² for ×1000);
- and dividing by the width of the zone (126 µm), with the two last operations being performed in a single step by simply multiplying the surface fraction by the height of the rectangular micrograph zone of interest.

This led to an equivalent thickness for the internal oxide.

Hardness evaluation

Vickers-mode macro-indentation was carried out to estimate the hardness of the six alloys for their three states: as-cast, aged 24 h at 1127°C and aged 24 h at 1237°C. A Testwell Wolpert indentation machine was used, and the test was performed with a 10 kg load (penetration progress for 5 seconds followed by dwell at a constant load for 10 seconds). Five Hv10kg results were obtained per sample, followed by the calculations of the average value and the standard deviation.

RESULTS

Chemical compositions and as-cast microstructures of the obtained alloys

The chemical compositions of the obtained alloys, determined via EDS on three ×250 zones randomly chosen in the 1127°C-aged samples, are displayed in Table 1 *(located at the end of the manuscript)*. The contents of Cr and Ta are well respected, although they appear to be more or less higher than expected for Ta in the NCT2 and NCT3 alloys (a classical phenomenon in EDS when Ta is present as carbides). The general microstructures of the six obtained alloys in their as-cast states are illustrated in Figure 1 by SEM/BSE micrographs taken with ×250 magnification. Obviously, they can be allocated to three categories: a single-phase alloy with significant Ta segregation without any precipitated particles (NCT0), four alloys with a single-phase matrix containing numerous interdendritic black and white particles (NCT1 to 4) and an alloy with a double-phase matrix and containing Ta-segregated interdendritic spaces (NCT5). The detailed micrographs taken at ×1000, presented in Figure 2, allow a more exhaustive description of the as-cast microstructures.

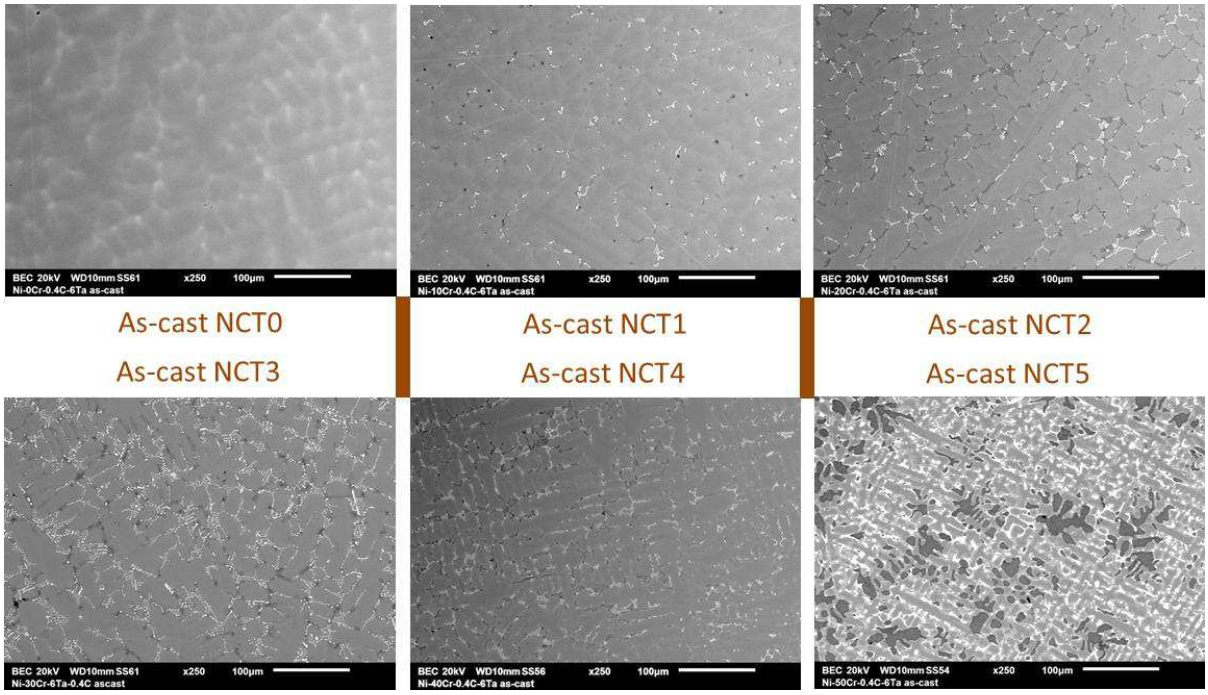

FIGURE 1. As-cast microstructures of the six obtained alloys (SEM/BSE micrographs, enlarged view: ×250)

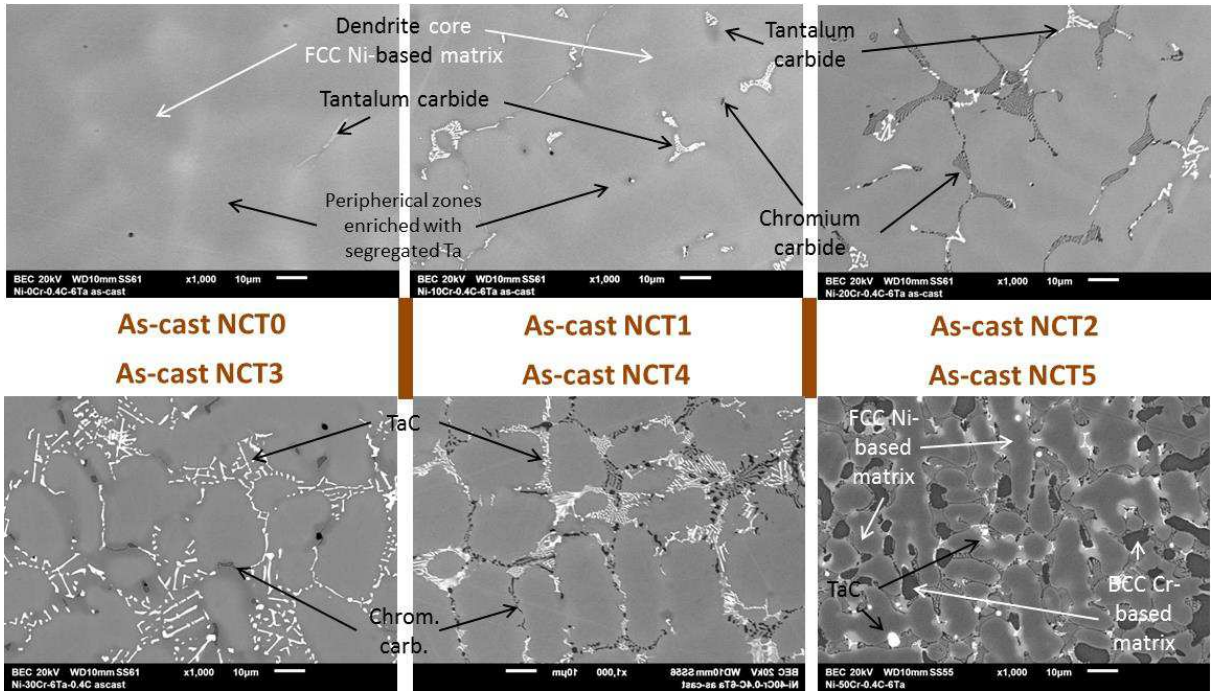

FIGURE 2. As-cast microstructures of the six obtained alloys (SEM/BSE micrographs, enlarged view: ×1000)

NCT0 is not really single phase because some rare and isolated white particles also exist. Their white tint, as well as their high concentration in Ta, confirmed by EDS spot analysis, suggests that these particles are tantalum carbides. However, due to their very small size, it is not possible to measure the carbon content. Similar to NCT0, the NCT1 alloy also presents matrix dendrites with a periphery clearer than the core, revealing here too significant segregation in tantalum during pre-eutectic matrix growth. Carbides, which are obviously of a eutectic nature (mixed with the matrix), are clearly TaC, as demonstrated by spot analyses carried out on the coarsest ones found in the microstructures. One can also note the presence of few small chromium carbides (darker than the matrix). These ones, obviously also eutectic, are much more present in the NCT2 alloy, in which the script-like eutectic TaC is also more developed than in the previous alloy. The acicular shape and the very dark tint of the chromium carbides suggest that they are of the Cr_7C_3 type, according to WDS results (wavelength dispersion spectrometry) previously obtained using a microprobe on identical particles found in cast alloys with similar chemical compositions. Although difficult to carry out, the EDS spot analyses performed on the coarsest dark carbides effectively suggest an atomic Cr/C ratio close to 2. The interdendritic carbide network is more developed in the NCT3 alloy, but the TaC carbides seem to be much more developed than the chromium carbides. These ones become more present again in the NCT4 alloy. The last alloy, NCT5, is very different from all the previous ones. In addition to a dendritic network of Ni solid solution matrices with interdendritic Ta-segregated zones and TaC carbides, many coarse dark areas are present. They are especially rich in Cr (60 wt.% and higher) and contain rather high Ni (36 wt.%) and Ta (3 wt.%) quantities. As suggested by the XRD spectrum given in Figure 3, these two main phases are face-centered cubic Ni-based and body-centered cubic Cr-based solid solutions. These constituents are the same as the ones found in the as-cast microstructure of Cr(bal.)-50 wt.% Ni alloy studied in a recent work [33]. Thus, the NCT5 alloy has the same microstructure as this binary alloy, but the NCT5 microstructures also contain interdendritic Ta-segregated zones and TaC precipitates.

Microstructure changes after 24 hours at 1127°C and 24 hours at 1237°C – qualitative observations

After 24 hours isothermally spent at 1127°C, all microstructures changed (Figure 4). This exposure acted as a homogenization treatment for the NCT0 alloy, in which the outer parts of dendrites rich in Ta subsequent to

segregation at solidification disappeared, as did the rare Ta-rich particles. The exposure to 1127°C induced the disappearance of the chromium carbides initially present in the NCT1 alloy. This 1127°C exposure also acted as a precipitation treatment because numerous secondary carbides appeared in the matrix. Such TaC precipitation also occurred in the NCT2 alloy, in which one can note the onset of both coalescence of the primary tantalum carbides and disappearance of chromium carbides. For the NCT3 alloy, which was already almost free of chromium carbides, the interdendritic network of script-like TaC is significantly affected: fragmentation and visible decreases in the surface fraction. The carbide population is shared between chromium carbides and tantalum carbides in the NCT4 alloy. Lastly, the microstructure of the NCT5 alloy, initially rather complex with many phases, some of which were chemically heterogeneous, became clearly simplified after exposure to 1127°C because it then was only double phase. Except for some small blocky TaC, the main phases present are the FCC Ni-based solid solution and the BCC Cr-based solid solution. Some fine particles of one of the phases can be found in the other one: this results from solid state precipitation during post-isothermal stage cooling, as previously observed in a binary Cr-50Ni (wt.%) alloy [33].

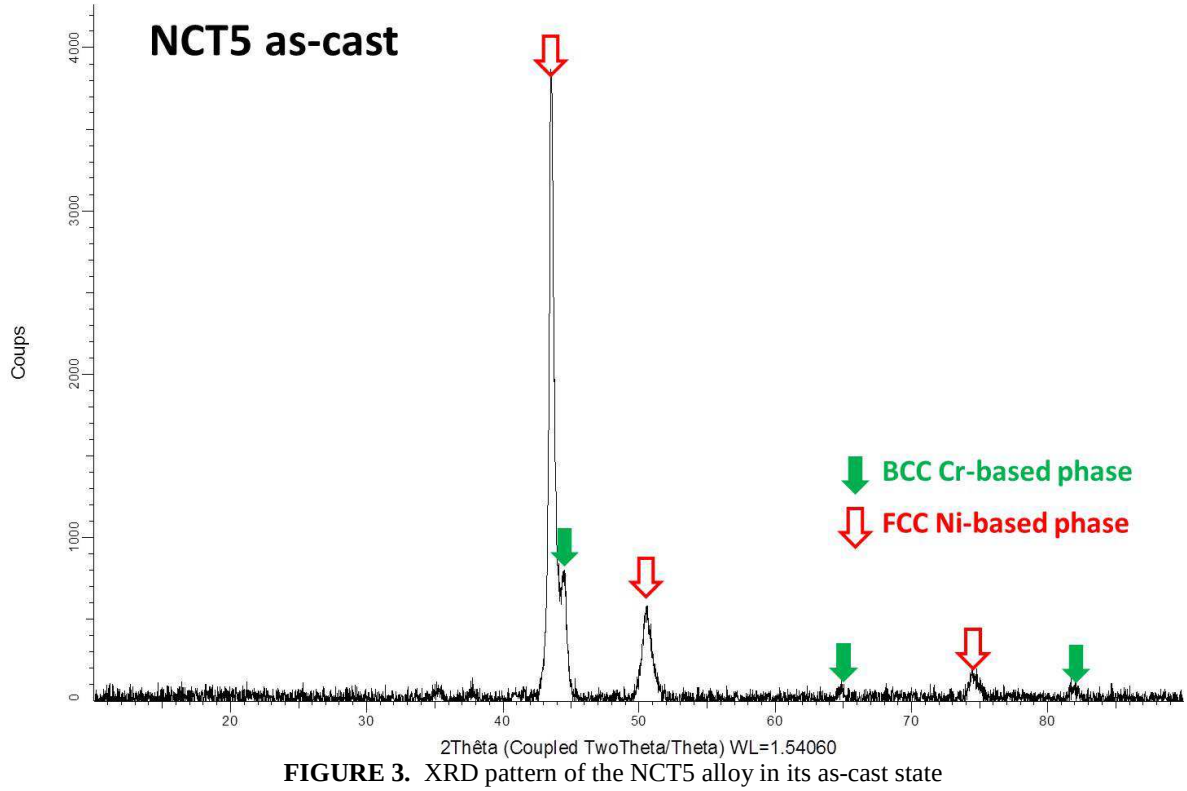

FIGURE 3. XRD pattern of the NCT5 alloy in its as-cast state

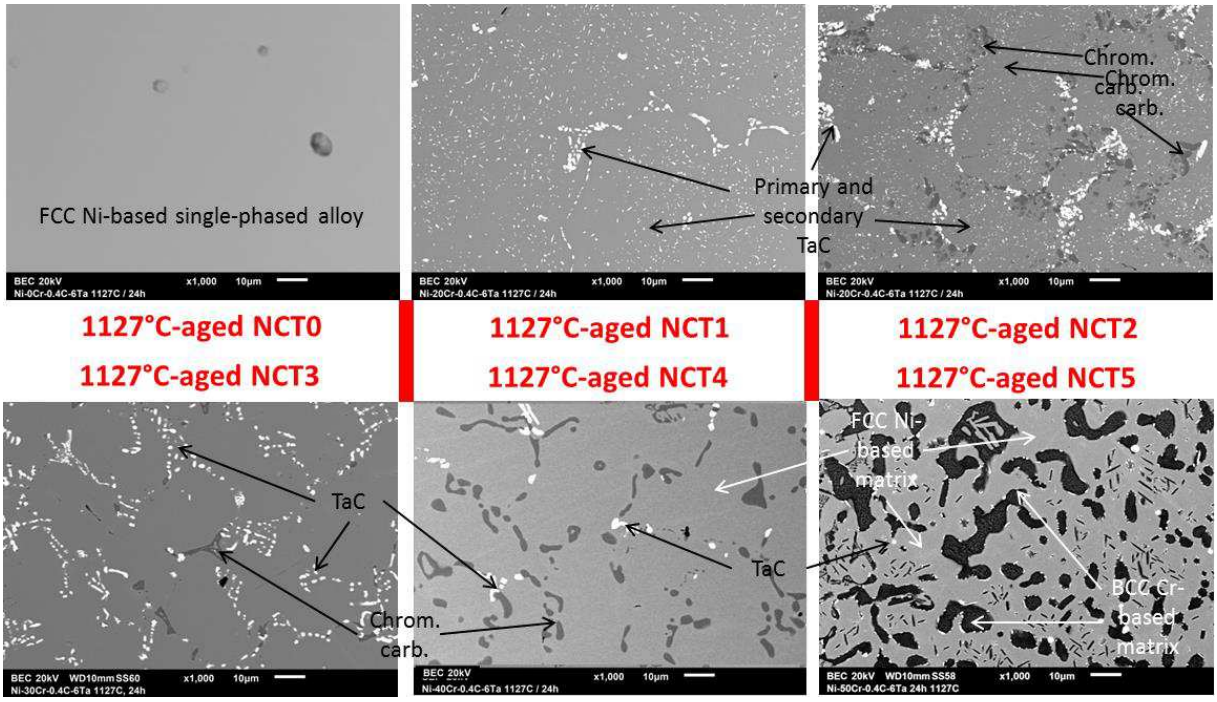

FIGURE 4. Microstructures of the six alloys after 24 h at 1127°C (SEM/BSE micrographs, enlarged view: ×1000)

After 24 hours at 1237°C, the microstructures unsurprisingly also evolved from the as-cast ones (Figure 5). In this case, not only the NCT0 alloy but also the NCT1 one became single phase, and this phase was still stable at 1127°C in the NCT1 alloy. At more than one hundred degrees higher, the TaC carbides were no longer stable, they became totally dissociated, and their constitutive atoms totally dissolved in the Ni-based solid solution. Concerning the NCT2, NCT3 and NCT4 alloys, the carbides present after aging are the same as those for 1127°C, but they are noticeably coarser and coalesced. The microstructure of the NCT5 alloy is not as simple as that after 24 h at 1127°C since TaC is more present.

Microstructure changes after 24 hours at 1127°C and 24 hours at 1237°C – quantitative results

The surface fraction of the carbides was measured on three ×1000 SEM/BSE micrographs by image analysis, and the results for all alloys and all states are plotted in Figure 6(A) for the chromium carbides (except for the NCT5 alloy, which does not contain such carbides) and Figure 6(B) for the tantalum carbides. These quantitative data,

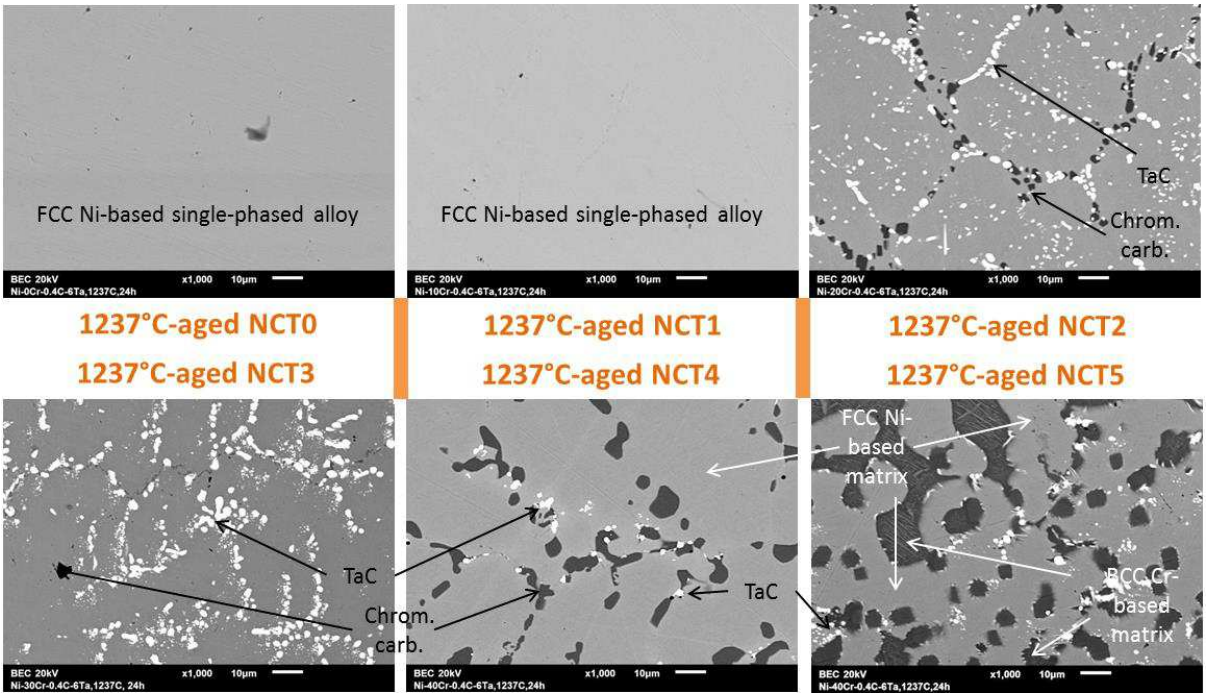

FIGURE 5. Microstructures of the six alloys after 24 h at 1237°C (SEM/BSE micrographs, enlarged view: ×1000)

which confirm the previous qualitative observations, allow us to see that aging may have had only a small effect on the chromium carbides in the NCT1 and NCT2 alloys (overlapping error bars), but it tends to decrease the surface fraction of the Cr_xC_y carbides (1127°C) and even suppress them (1237°C). In contrast, a huge increase in the surface fraction of chromium carbide occurs for the NCT4 alloy. One must note here that EDS spot analyses confirm that these regions are chromium carbides and not a BCC Cr-based phase. Contrasting effects on the TaC surface fraction were also observed among the alloys: one day of high temperature aging induces a surface fraction decrease and evendisappearance of TaC for the NCT1, NCT4 and NCT5 alloys, while the opposite effect is noted for the NCT2 and NCT3 alloys. The total quantity of carbides of all natures can be of great interest. The surface fractions of chromium carbides and the surface fractions of tantalum carbides were then added together, and the obtained values are plotted in the graph presented in Figure 7. This one clearly shows a jump in carbide quantity as soon as the chromium content becomes sufficiently high (NCT2 to NCT4 alloys, by comparison to the NCT0 and NCT1 alloys). One can also observe a drop for the NCT5 alloy and its double-phase matrix.

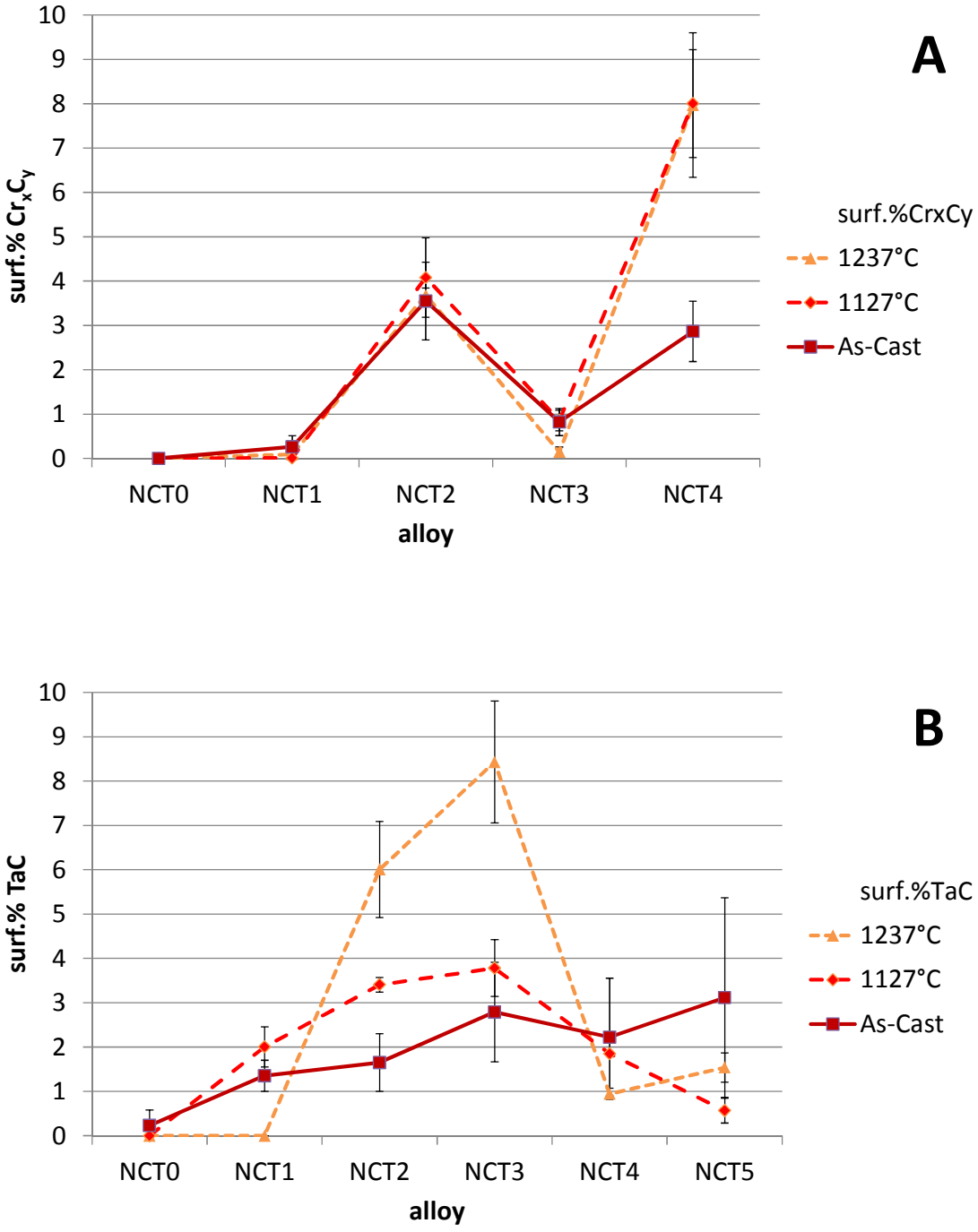

FIGURE 6. Surface fraction of the chromium carbides (A) and of the tantalum carbides (B) in all alloys for all their metallurgical states (as-cast and 24 h-aged at 1127°C and at 1237°C)

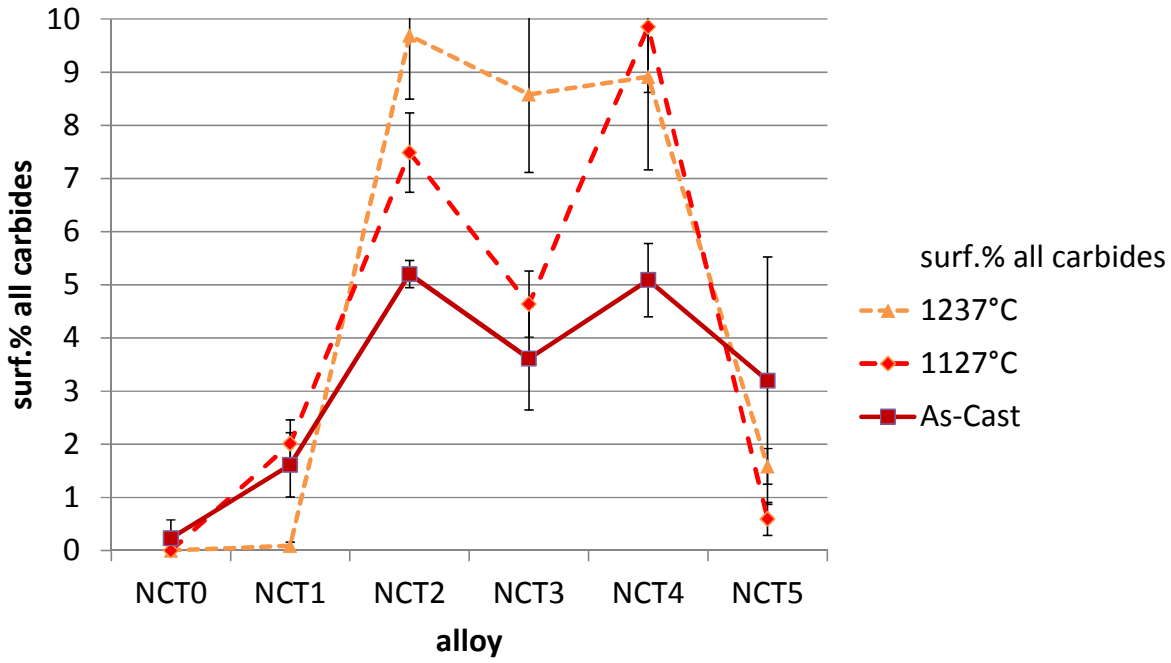

FIGURE 7. Total surface fraction of the carbides in all alloys for all their metallurgical states (as-cast and 24 h-aged at 1127°C and at 1237°C)

The two graphs displayed in Figure 8 show how the chromium (A) and tantalum (B) weight contents in the matrix evolve from the NCT0 alloy to the NCT5 alloy and from the as-cast state to the aging at the highest temperature. In addition to the unsurprising increase of the Cr content in the matrix with the increase in Cr in the alloy, one can see in the first graph that the Cr content in the matrix tends to increase with the aging temperature for the NCT3 alloy (consistent with the small decrease in chromium carbides that was previously noted) and to decrease with aging for the NCT4 alloy (consistent with the increase in the chromium carbide fraction seen before). The greatest variation in the Cr content in the matrix is observed for NCT5, for which the decrease in Cr, measured in the nickel-based matrix again, is due to the presence of the second part of matrix, the BCC Cr-based one. Concerning the Ta content in the matrix, its decrease (respectively increase) is more or less correlated with the increase (resp. decrease) in the TaC surface fraction for the NCT1 to NCT3 (resp. NCT4 and NCT5) alloys. It is true that the result dispersion (see the standard deviation value or error bar length) is particularly important in some cases.

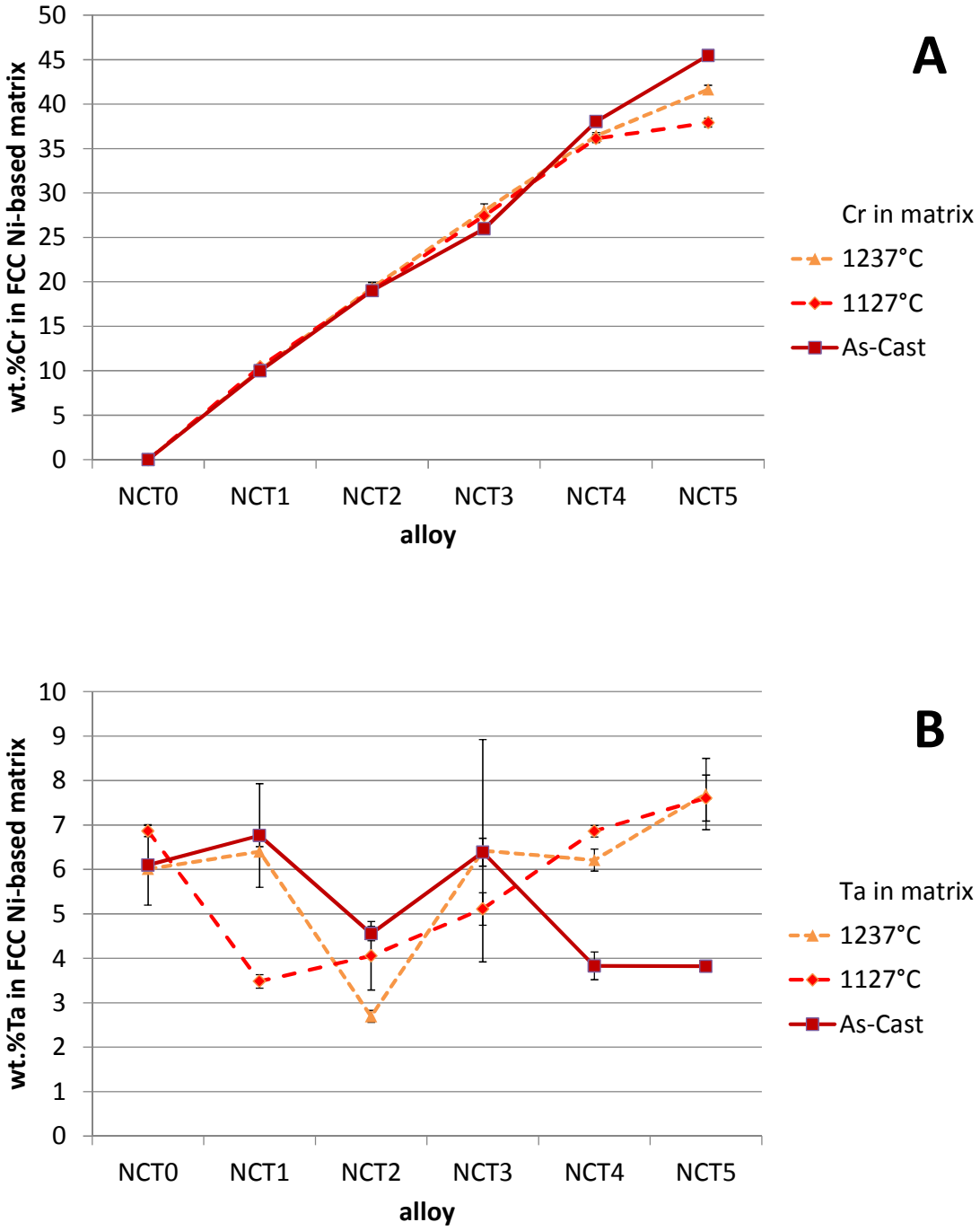

FIGURE 8. Weight contents of chromium (A) and tantalum (B) in the FCC Ni-based matrix of all alloys for all their metallurgical states (as-cast and 24 h-aged at 1127°C and at 1237°C)

Hardness

The hardness dependence on the Cr content in the alloy and on the metallurgical state is illustrated in Figure 9. One can see that the reproducibility of the indentation results is rather good. The average hardness increases rather regularly from the NCT0 alloy to the NCT5 alloy. This increase in hardness with the chromium content in the alloy can be logically attributed to the increase in the carbide fraction by considering only the five first alloys (NCT0 to NCT4). However, a contribution from the Cr enrichment of the FCC Ni-bases matrix is also expected: indeed, it was observed that the hardness of Cr-containing Ni-based cast alloys may slightly increase with the Cr content, from 70 to 160 Hv_{30kg} from 0 to 35wt.% Cr [34]. In contrast, another explanation must be found for the significant jump in hardness seen for the NCT5 alloy, i.e., the appearance of the BCC Cr-based matrix part. Indeed, it was earlier observed that the Ni-saturated BCC Cr-based phase present in Cr-Ni binary alloys containing more than 50 wt.% Cr presents a very high hardness, near 760 Hv_{10kg} [33]. In the same work, it was found that hardness was decreased by high temperature aging, an effect that was enhanced when the aging temperature was higher. This is a classical consequence of the fragmentation of the carbides, which deviated from their initial shapes inherited from the fine solidification mechanisms that governed their growth.

Oxidation state after exposure to 1127°C and 1237°C– qualitative observations

After 24 hours spent at 1127°C in air, all samples were more or less oxidized on the surface and in the subsurface. The most oxidized one is logically the chromium-free one: NCT0. By looking at the cross-sectional SEM/BSE micrographs given in Figure 10, one can see that oxidation growth acted both outwards and inwards. This is also clearly evidenced by the absence (outer part of the oxide scale) or presence (inner part) of tantalum-rich particles mixed with the oxide scale. The outer part of the oxide scale is composed of NiO oxide only, as specified by SEM/EDS spot analyses. The gray area of the inner part is mainly composed of NiO and more or less elongated particles rich in Ta. These oxides seem to be tantalum oxides (Ta_2O_5), but they are all too small to allow analyses to be accurate enough to confirm this identification. The NCT1 alloy presents more classical surface and subsurface oxidation features, which are systematically found after high temperature oxidation of Cr-rich and Ta-containing alloys: an outer oxide scale made of chromia in which dispersed small particles rich in Ta are also present. A sub-

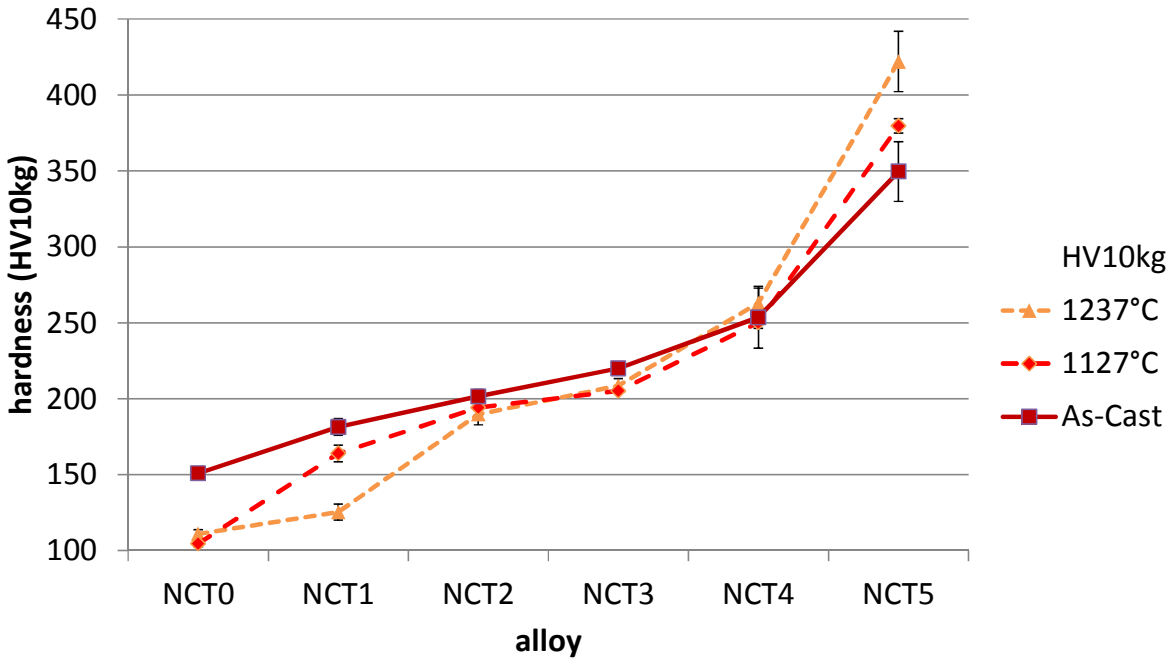

FIGURE 9. Hardness of all alloys in all their metallurgical states (as-cast and 24 h-aged at 1127°C and at 1237°C); average and standard deviation from 5 indentations

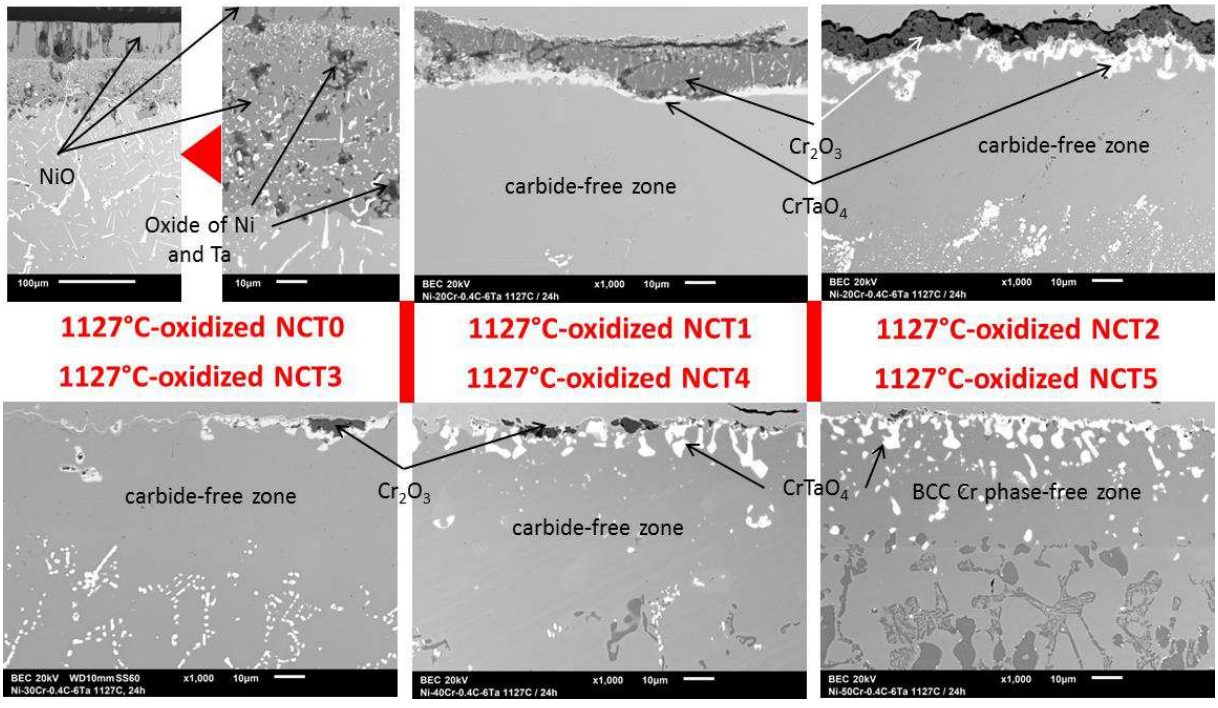

FIGURE 10. Surface states of the six alloys after 24 h at 1137°C in laboratory air (SEM/BSE micrographs, ×1000)

layer of $CrTaO_4$, a classical oxide, is also present at the interface separating the chromia scale and the alloy. Deeper, a zone of alloy having obviously lost its initial carbides has developed. Here, only the matrix is present because the TaC has dissolved. The Ta and C atoms that these carbides involved have dissolved in the neighboring matrix. At the same time, this matrix tended, in contrast, to be impoverished in these same elements by another phenomenon: Ta and C simultaneously diffused toward the oxidation front to be oxidized (as chromia and the subsurface oxide $CrTaO_4$). Deeper again, one finds bulk-type microstructures composed of matrix and carbides. As described above, these fractions are coarsened and fragmented, and their surface fractions have changed. The same qualitative observations, comments and interpretations can be made for NCT2 to NCT4, except that the outer chromia scale has obviously spalled off almost totally during cooling for the NCT3 and NCT4 alloys. This resulted in the presence of isolated small areas of chromia here and there on the alloy, instead of a real scale. In the specific case of the NCT5 alloy, which was initially different from the five other alloys because of the constitution of its matrix, one should note that this exhibited the BCC Cr-based phase, which disappeared in the subsurface. This phase acted as a chromium reservoir, and its dissolution released Cr atoms, which diffused and participated in the constitution and maintenance of the outer chromia scale. Tantalum has itself also significantly diffused in the outward direction, and it oxidized as internal oxides with the inward diffused oxygen. It also participated in the formation of the sub-chromia $CrTaO_4$ oxide.

After 24 hours at 1237°C (Figure 11), the surface and sub-surface consequences of oxidation are globally the same, with the main differences being the greater thickness of the oxide scale and the greater depth of the carbide-free zone (or of the subsurface zone free of the BCC Cr-phase in the case of the NCT5 alloy). This is the reason for the choice of two magnifications for the presented micrographs: ×250 for a general view, allowing the carbide-free zone and part of the still carbide-containing bulk to be seen well, and ×1000 for a more detailed view of the oxides.

Oxidation state after exposure to 1127°C and 1237°C – quantitative results

The first quantitative data of interest was logically the quantity of oxides formed. However, it was not possible in many cases to specify the thickness of chromia because the scale spalled off for all the chromia-forming alloys and the two temperatures. One can just mention the thickness of the external chromia (approximately 10 µm), the measurement of which was possible for the NCT1 and NCT2 alloys after oxidation at 1127°C. These thicknesses of

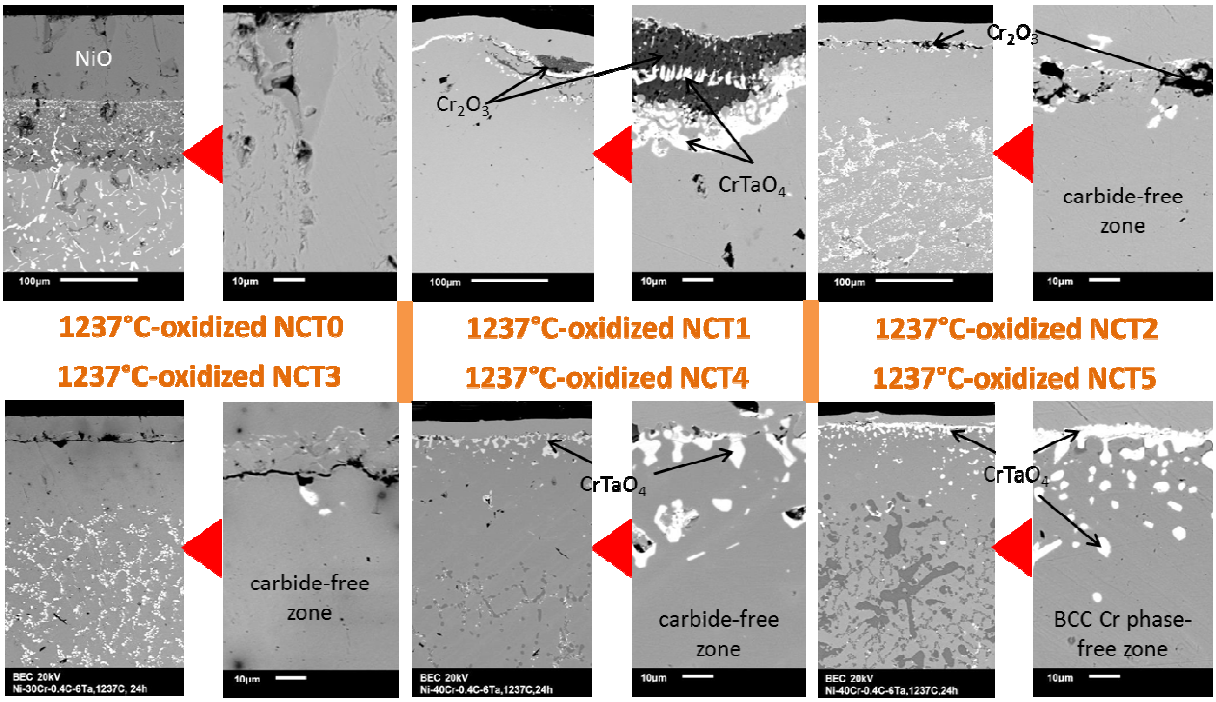

FIGURE 11. Surface states of the six alloys after 24 h at 1237°C in laboratory air (SEM/BSE micrographs, ×250 and ×1000)

the external chromia scale are much lower than those of the NiO oxide grown externally (approximately 50 µm) and the NiO internal oxide (approximately 60 µm) mixed with tantalum oxides developed in the Cr-free NCT0 alloy at the same temperature by cationic diffusion and anionic diffusion, respectively. At 1237°C, the thicknesses of these two parts of the NiO oxide are twice those at 1127°C.

Not subjected to spallation since it was well attached to the outermost part of the alloy with which it was mixed, the $CrTaO_4$ oxide was analyzed in a quantitative manner. This was done using image analysis for the surface fraction measurements, which were thereafter expressed in terms of equivalent thickness (method described in the experimental details section). The obtained equivalent $CrTaO_4$ thicknesses are graphically given in Figure 12. The alloy presenting the greatest $CrTaO_4$ equivalent thickness is logically the NCT0 alloy. Indeed, it oxidized much faster than the other ones, taking into account the absence of chromium and the consequently fast growth of NiO. Notably, the significant depth of inward growth of NiO exposed many tantalum atoms to internal oxidation (in Ta_2O_5), not only in the matrix zone converted into NiO oxide but also much deeper.

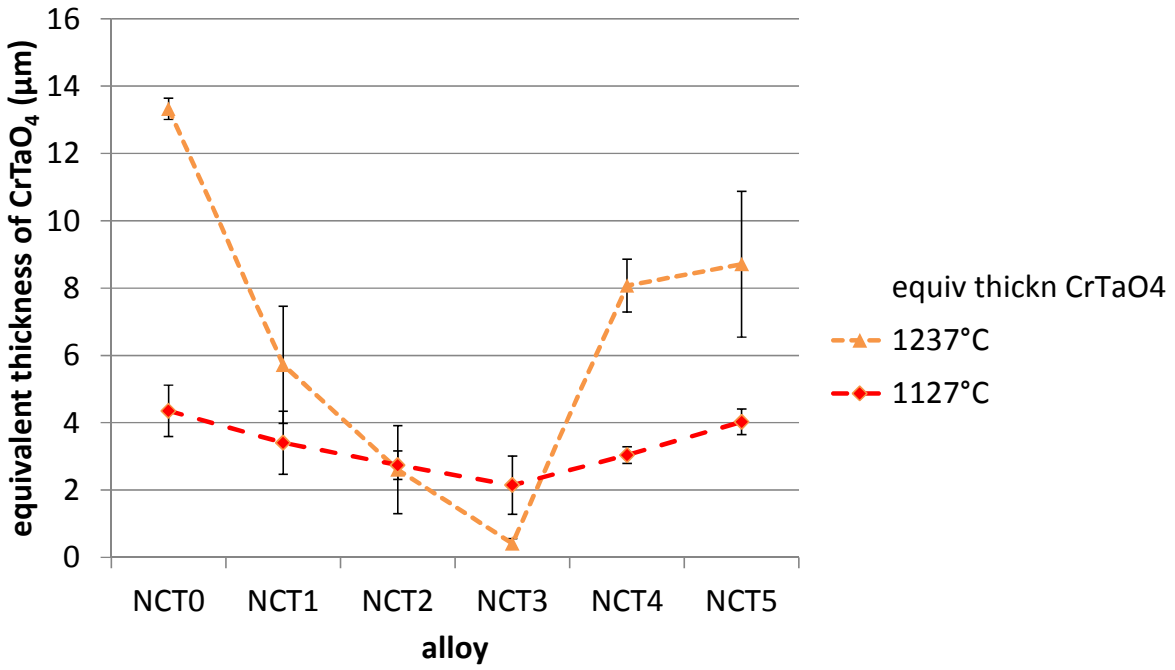

FIGURE 12. Equivalent thickness of the $CrTaO_4$ oxide present in the subsurface close to the oxidation front for the six alloys after 24 h at 1127°C and at 1237°C in laboratory air

Obviously, the inward diffusion of the small oxygen atoms predominated over the outward diffusion of the less mobile large tantalum atoms. The equivalent thickness of Ta_2O_5 formed at 1237°C is three times that obtained for 1127°C. This logical difference is found again for the NCT1 alloy, but with a lower ratio. Owing to a protective external layer of chromia, oxygen did not access the Ta atoms present in this alloy, in solid solution (at 1127°C or 1237°C) or in TaC carbides (1127°C only). Instead, Ta diffused outward, as for the other alloys. The equivalent $CrTaO_4$ thicknesses are minimal for the NCT2 and NCT3 alloys, certainly because of better protection by the external chromia scales. Indeed, these alloys are of better quality due to the efficient supply of Cr for these alloys rich enough in this element. Curiously, the equivalent $CrTaO_4$ thickness increases from NCT3 to NCT4. This difference between the two alloys may be explained by the difference in the carbide population in the as-cast state as well as during exposure to high temperature: tantalum seems more stable in the NCT3 alloy because it is associated with carbon in carbides, while a greater proportion of Ta is present as mobile atoms in solid solution in the NCT4 alloy, which contains less TaC and more chromium carbides. Even if the oxidation of tantalum initially belonging to TaC carbides is possible (see the cases of NCT2 and NCT3, in which carbide-free zones developed), this supposes dissociation into Ta and C first and diffusion of the released Ta atoms second. Principally in the NCT0 alloy, but

also partly for the NCT4 alloy, the first step is already realized before the oxidation test. Lastly, concerning the last alloy, NCT5, which initially also contains only rare TaC, tantalum has also only to diffuse toward the oxidation front, resulting in an increase in the equivalent $CrTaO_4$ thickness.

The oxidation processes led to the oxidation of both chromium and tantalum diffusing from the bulk over an increasing depth. This involved first the atoms present in the solid solution but, shortly after, also the Cr-rich and Ta-rich particles, which started decomposing to allow the local thermodynamic equilibrium to be achieved despite the impoverishment in Cr and Ta of the foreign matrix. This subsurface destabilizing effect of oxidation led to the progressive development of a carbide-free zone from the interface between the alloy and the external oxide. This concerned only the NCT1 to NCT4 alloys, which contained carbides in fractions high enough. The evolution, versus the chromium content in the alloy, of the carbide-free depth as measured on SEM/BSE cross-sectional micrographs is plotted in Figure 13. One can see that the carbide-free zones are the deepest in the case of the NCT1 alloy, which initially contained a low fraction of carbides, at 1127°C and at 1237°C. The point corresponding to this alloy oxidized at 1237°C corresponds to a part of the subsurface where rare carbides were observed; in contrast, carbides were totally absent in other core regions. The carbide-free depths are lower for the NCT2 to NCT4 alloys for the two aging temperatures because of the presence of much more carbides in these alloys. However, the NCT4 alloy, in which a great portion of the carbides initially present was composed of chromium carbides at high temperature, was more affected by the development of a carbide-free zone than the NCT2 and NCT3 alloys, in which the carbide populations were mainly composed of TaC. Concerning the NCT5 alloy, it is not a carbide-free depth that was measured but the depth of the disappearance of the BCC Cr-phase in the subsurface. Very rich in chromium, this depth is logically less extended than many of the carbide-free depths measured for all the alloys.

To finish with the quantitative exploration of the oxidation effects, one can look at the Cr impoverishment in the extreme surface. The Cr weight contents specified by SEM/EDS spot analysis in the alloy in locations very close to the oxidation front are graphically given in Figure 14. One can see that from the NCT1 alloy to the Cr-richest NCT5 alloy, the Cr content in the extreme surface is approximately 6-7 wt.% lower than initially (initial contents given by the “as-cast” curve). This occurs without any consequence for the chromia-forming behavior of the NCT5 to NCT3 alloys. This is also true for the NCT2 one, despite it commonly being considered that 20 wt.% Cr is the bottom limit for a nickel-based alloy to remain chromia forming. Indeed, the NCT2 alloy obviously maintained its chromia-

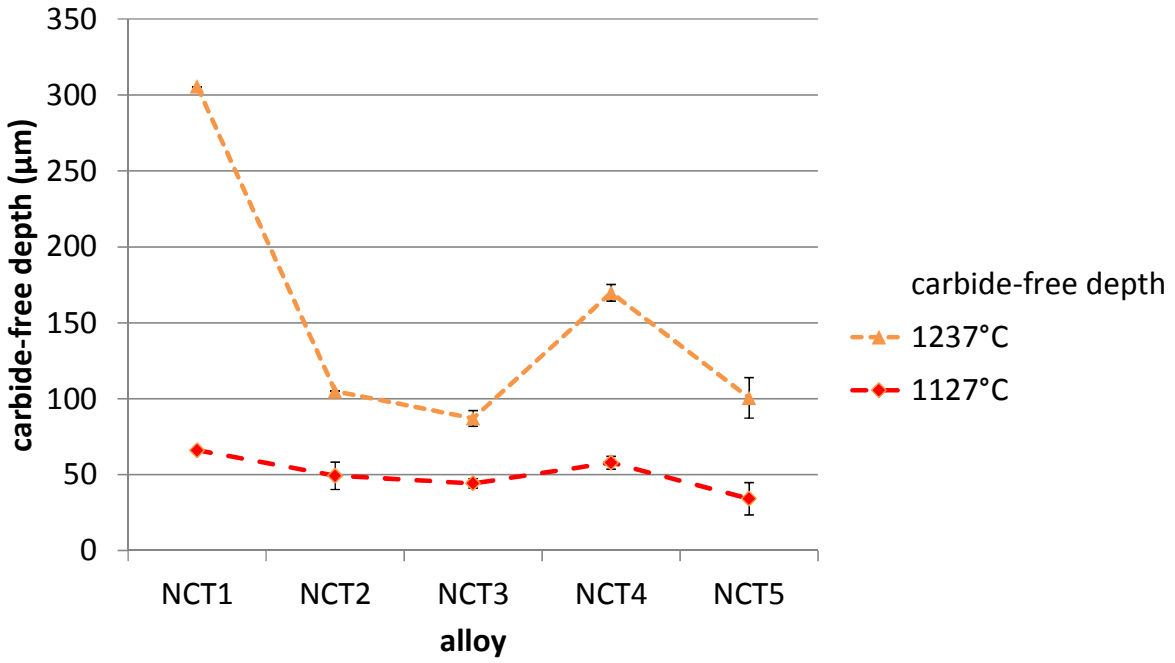

FIGURE 13. Carbide-free depth (or depth of the disappearance of the BCC Cr-phase in the case of NCT5) of the six alloys after 24 h at 1127°C and at 1237°C in laboratory air

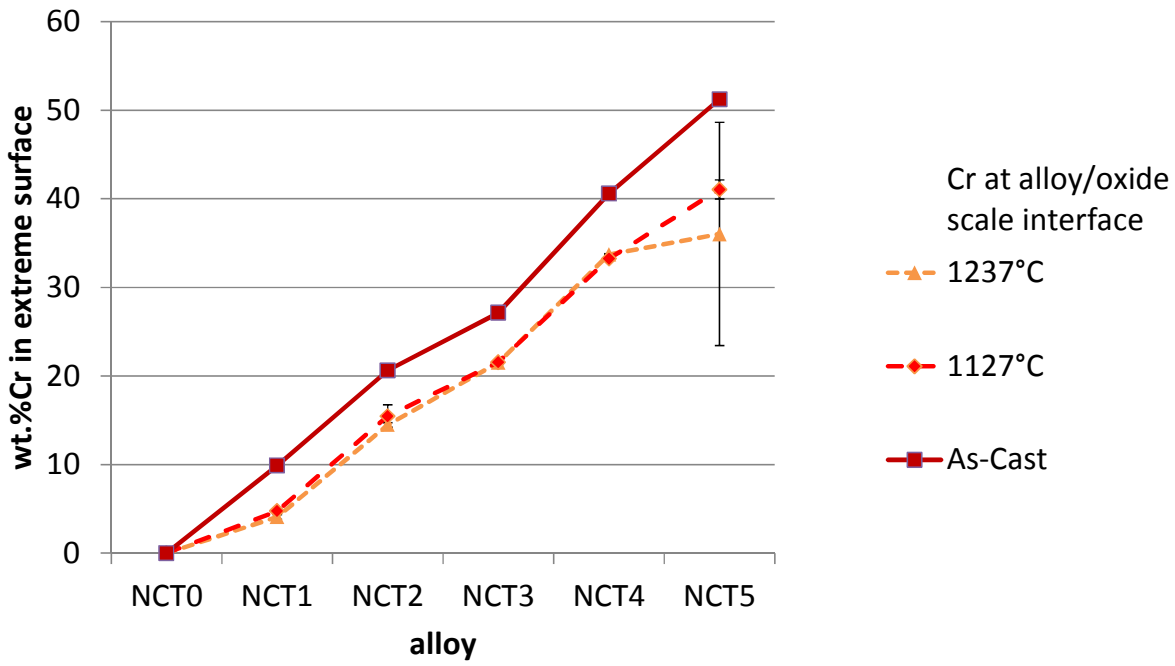

FIGURE 14. Chromium weight content in the subsurface very close to the oxidation front for the six alloys after 24 h at 1127°C and at 1237°C in laboratory air

forming ability until the ends of the oxidation experiments. In contrast, the NCT1 alloy, which did not initially respect the {Cr > 20 wt.%}-rule, contained only approximately 5 wt.% Cr in the extreme surface after 24 hours; it was certainly threatened by imminent catastrophic oxidation.

DISCUSSION

The first comments may be made about the bulk microstructures of these six alloys, the ones obtained after solidification and post-solidification cooling and the ones stabilized at 1127°C or 1237°C. Taking into account their relative proximity to the liquidus temperatures preliminarily assessed with Thermo-Calc (from 1420°C for the NCT0 alloy to 1306°C for the NCT5 one), the 24 hours of exposure to these temperatures can be considered as long enough to reach the thermodynamic equilibria. The variation in the chromium content in a {Ni(bal.)-0.4C-6Ta}-based cast alloy had important consequences on the as-cast microstructures and the ones stabilized at high temperature. The case of the Cr-free NCT0 alloy is very particular: by suppressing Cr in the chemical composition of the alloy, it was astounding to observe the total absence of carbides. Despite the very low Gibbs energy of the TaC phase (-34,900 + 0.5 × T cal / mol of C between 1250 and 1400 K versus -12,833 – 3.05 × T cal / mol C for chromium carbides [35]), tantalum did not profit from the absence of its carbide-forming challenger to appear in great quantities. In contrast, tantalum stayed in the solid solution in the matrix as though chromium allowed it to substitute for nickel on the sites of the crystalline structure. Obviously, in a Cr-free Ni-based matrix, the most stable position of tantalum is in substitution for the base element in the matrix, even if carbon is available to form carbides. With the presence of 10 wt.% Cr in the NCT1 alloy, it seems that there is not enough sites to accept all the Ta atoms in the solid solution, and some of them must form some TaC carbides. In this NCT1 alloy as well, chromium is present in a quantity low enough to stay almost totally in the solid solution. With another 10 wt.% Cr increase (NCT2 alloy), a greater proportion of TaC is present, and chromium carbides are now really present in the as-cast microstructure. By increasing the Cr content (NCT3 and NCT4), rather high fractions of TaC and chromium carbides are present. Enriching more in chromium induces the appearance of a second type of matrix phase, a Cr-based phase. This one is saturated in nickel, and its crystalline structure is body-centered cubic. Twenty-four hours of aging at 1127°C was sufficient to totally homogenize the NCT0 alloy. Logically, 24 hours at 1237°C led to the same result. The total disappearance of the TaC carbides initially present in the NCT1 alloy was achieved after 24

hours at 1237°C: obviously, this temperature is high enough to allow the matrix to host all chromium, tantalum and carbon atoms in solid solution. In contrast, this was not possible at 1127°C, as demonstrated by the presence of TaC carbides, primary and secondary (precipitated during the high temperature stage). When the chromium content is equal to 20 wt.% or higher, it is not possible to keep the Cr, Ta and C atoms in solid solution, even at 1237°C. Chromium carbides and tantalum carbides co-exist. The former ones tend to be significantly more present when the chromium content in the alloy increases beyond the 30 wt.% Cr of the NCT3 alloy, which contains the highest TaC fraction at the expense of the chromium carbides. Thus, as it was earlier thought that chromium tends to hinder the formation of TaC in Ni-Cr alloys, in which chromium carbides seemed favored despite the stronger carbide-forming power of tantalum, this phenomenon is not so simple. In fact, it may be more the high, but limited, capacity of the austenitic nickel matrix to host high contents of Cr and Ta simultaneously that is responsible for the lack of tantalum carbides in nickel-based alloys despite the presence of tantalum and carbides in similar molar quantities. Furthermore, the Ta/Cr balance for the tantalum and chromium quantities stored in the solid solution seems to be higher in the case of nickel than in the case of cobalt and iron [24, 27, 28]. One can finish the discussion concerning the bulk microstructures and the evolution of the carbide population by noting that these results can be associated with other studies dealing with the thermodynamic stability or thermal evolution of chromium carbides [36], MC carbides [37], and both when present together [38, 39]. These recently published works do not address competition between chromium carbides and tantalum carbides, but they all demonstrate the current interest for the relative stabilities at high temperatures of different types of carbides in the alloys that they are devoted to strengthening.

Concerning the consequences of the changes in the chromium content for the behavior of the alloys under oxidation at high temperature, it was not surprising to observe a significant deterioration when the Cr content in the alloy was rated at values less than 20 wt.%: fast NiO growth for the NCT0 alloy with internal oxidation of Ta, as well as chromia-forming behavior for the NCT1 alloy but imminence of catastrophic oxidation. Only the alloys rich enough in Cr behaved well, even the {double matrix}-containing NCT5 alloy. In addition, the quantitative investigation of the oxidation of Ta using image analysis to assess the equivalent $CrTaO_4$ thickness revealed a possible easier internal oxidation of Ta when present in solid solution than when associated with carbon in the TaC carbides. One can note again, as earlier observed for other alloys rich in tantalum, that the development of the sub-chromia $CrTaO_4$ scale was deleterious for the adherence of the external oxide scale on the substrate, leading to

severe spallation upon cooling, which did not allow an extensive characterization of the chromia scale in terms of quality (compactness and absence or presence of pores and cracks) and of average thickness.

CONCLUSION

The first contribution from the knowledge of this study is the difficulty of making better than the classical Ni-30Cr-0.4C-6Ta in terms of the TaC population by varying the Cr content; 0.4% C and 6% Ta with 30% Cr are weight contents high enough to promote the formation of carbides with fractions high enough to efficiently strengthen the alloy but not too high for preserving the discontinuity of the interdendritic carbides network to maintain ductility and fracture toughness. With regard to this reference, one cannot obtain more high-temperature-stable TaC by decreasing the Cr content in the alloy (this destabilizes a portion of the TaC) or by increasing it (this favors a higher chromium carbide / TaC ratio).

A second contribution is the knowledge of the dependence of the high temperature oxidation behavior of the studied Ni-Cr-0.4C-6Ta base of the alloy on the chromium content, with notably the minimum Cr content recommended. A problem of easy oxide scale spallation upon cooling due to the unavoidable formation of $CrTaO_4$ at the interface was also evidenced, a phenomenon that may be obstructed by additions of yttrium to peg the chromia scale on the alloy substrate.

A third contribution is the discovery of the as-cast and aged microstructures of several versions of a Ni-Cr-C-Ta alloy different from one another in terms of the Cr content level (for a rather wide Cr interval). Notably, the characterization of the stable states for the two considered temperatures produced qualitative and quantitative data (number and identities of the phases, their fractions and their individual compositions) useful for testing thermodynamic calculations. Morphologic results may be useful for other considerations.

Further work to try to obtain a carbide population composed only of TaC, with a script-like shape imbricated with the matrix to enhance their strengthening effect, may consist of increasing the Ta content beyond the 6 wt.% of the present alloys and decreasing the Cr content below 20 wt.%, for example, with a carbon content maintained at 0.4 wt.% C. However, other methods can be tested by escaping from the quaternary Ni-Cr-C-Ta system, for example, by adding moderate quantities of base elements possibly favorable to a better stability of the TaC carbides at the expense of chromium carbides – for example, Co and Fe – as suggested by previously obtained recent results.

Acknowledgments

The author wishes to thank Miss Zohra Himeur, Master's student in the trainee period who helped him technically in this work.

References

[1] M. J. Donachie, S. J. Donachie: *Superalloys: A Technical Guide*, 2nd ed., ASM International, Materials Park, 2002, pp. 79-90.

[2] M. Durand-Charre: *The microstructures of Superalloys*, CRC Press, Boca Raton, 1997, pp. 10-11.

[3] D. Young, *High Temperature Oxidation and Corrosion of Metals*, Elsevier, 2008, pp. 34-37.

[4] P. Kofstad, *High Temperature Corrosion*, Elsevier Applied Science, London, 1988, pp. 370-371.

[5] J. Di Martino: *Oxidation at High Temperature and Corrosion by the C_3 molten glass of Superalloys based on Cobalt*, Ph.D. thesis, Henri Poincaré University, Vandoeuvre-lès-Nancy, 2002, pp. 14-15.

[6] S. Michon: *Metallurgical and Mechanical Optimization of Cobalt-based Superalloys for Glass-forming Uses at 1200°C*, Ph.D. thesis, Henri Poincaré University, Vandoeuvre-lès-Nancy, 2004, pp. 73-78.

[7] C. T. Sims, W. C. Hagel: The Superalloys, John Wiley & Sons, New York, 1972, pp. 52-55.

[8] E. F. Bradley: Superalloys: A Technical Guide, ASM International, Metals Park, 1988, pp. 39-40.

[9] O. Renck, P. Ghosh and R. Pippan: *Scripta Materialia*, 2017, 137, pp. 60-63.

[10] Z. Wang, Y. Yuan, K. Arshad, J. Wang, Z. Zhou, J. Tang, G.-H. Lu: *Fusion Engineering and Design*, 2017, 125, pp. 496-502.

[11] Y. Mu, H. Liu, Y. Liu, X. Zhang, Y. Jiang and T. Dong: Journal of Alloys and Compounds, 2017, 714, pp. 668-680.

[12] C. Mathiou, A. Poulia, E. Georgatis and A. E. Karantzalis: Materials Chemistry and Physics, 2017, in press.

[13] X. Feng, J. Zhang, Z. Xia, W. Fu, K . Wu, G. Liu and J. Sun: Materials Letters, 2018, 210, pp. 84-87.

[14] F. Körmann, A. V. Ruban and M. H. F. Sluiter: Materials Research Letters, 2017, 5(1), 35-40.

[15] N. D. Stepanov, N. Y. Yurchenko, S. V. Zherebtsov, M. A. Tikhonovsky and G. A. Salishchev: Materials Letters, 2018, 211, pp. 87-90.

[16] L. Lilensten, J.-P. Couzinié, J. Bourgon, L. Perrière, G. Dirras, F. Prima and I. Guillot : Materials Research Letters, 2017, 5(2), pp. 110-116.

[17] H. Jiang, K. Han, D. Qiao, Y. Lu, Z. Cao and T. Li: Materials Chemistry and Physics, 2017, in press.

[18] Y. T. Xu, Q.-Z. Sha and T.-D. Xia: Zhongguo Youse Jinshu Xuebao, 2016, 26(2), pp. 302-309.

[19] Y. Guo, F. Zhong, Y. Yu, S. Li and J. Sha: Journal of Alloys and Compounds, 2017, 710, 725-735.

[20] L. Karge, R. Gilles, D. Mukherji, P. Strunz, P. Beran, M. Hofmann, J. Gavilano, U. Keiderling, O. Dolotko, A. Kriele, A. Neubert, J. Rösler and W. Petry: Acta Materialia, 2017, 132, pp. 354-366.

[21] R. Steinitz: *Jet Propulsion*, 1955, 25, pp. 326-330.

[22] G. W. Meetham, M. H. Van de Voorde, Materials for High Temperature Engineering Applications, Springer, 2012, p. 83.

[23] J. Di Martino, S., L. Aranda, P. Berthod, R. Podor and C. Rapin: *Annales de Chimie – Sciences des Matériaux*, 2003, 28 (Suppl. 1), pp. S231-8.

[24] P. Berthod, S. Michon, J. Di Martino, S. Mathieu, S. Noël, R. Podor and C. Rapin: *Calphad*, 2003, 27(3), pp. 279-88.

[25] S. Michon, P. Berthod, L. Aranda, C. Rapin, R. Podor and P. Steinmetz: *Calphad*, 2003, 27(3), pp. 289-94.

[26] S. Michon, L. Aranda, P. Berthod and P. Steinmetz: *La Revue de Métallurgie – C.I.T. / Science et Génie des Matériaux*, 2004, 9, pp. 651-62.

[27] P. Berthod, Y. Hamini, L. Aranda and L. Héricher: *Calphad*, 2007, 31(3), pp. 351-60.

[28] P. Berthod, L. Aranda, C. Vébert and S. Michon: *Calphad*, 2004, 28(2), pp. 159-166.

[29] L. Zheng, C. Gu and G. Zhang: Xiyou Jishu Cailiao Yu Gongcheng, 2005, 34(2), pp. 194-198.

[30] X. Z. Qin, J. T. Guo, C. Yuan, J. S. Hou and H. Q. Ye: Materials Letters, 2008, 62, pp. 2275-2278.

[31] K. Zhao, Y. H. Ma, and L. H. Lou: Journal of Alloys and Compounds, 2009, 475, pp. 648-651.

[32] L. Zheng, G. Zhang, T. L. Lee, M. J. Gorley, Y. Wang, C. Xiao and Z. Li: *Materials & Design*, 2014, 21, pp. 61-9.

[33] E. Conrath and P. Berthod: *Materials at High Temperature*, 2016, 33(2), pp.189-197.

[34] P. Berthod, E. Conrath: *Materials Science: An Indian Journal*, 2015, 13(11), pp. 347-352.

[35] S. R. Shatynski: *Oxidation of Metals*, 1979, 13(2), pp. 105-118.

[36] Z. Li, H. Mao, M. Selleby: *Calphad*, 2017, 59, pp. 107-111.

[37] Y. Liu, Y. Jiang, R. Zhou, J. Feng : *Journal of Alloys and Compounds*, 2014, 582, pp. 500-504.

[38] D. L. Shu, S. G. Tian, N. Tian, J. Xie, Y. Su, *Materials Science and Engineering A*, 2017, 700, pp. 152-161.

[39] L. Zhang, H. Liu, X. He, R. Din, X. Qu, M. Qin, Z. Li, G. Zhang, *Materials Characterization*, 2012, 67, pp. 52-64.

TABLES

TABLE 1. Chemical compositions of the alloys as obtained; average and standard deviation values coming from three EDS full frame measurements (carried out at ×250, i.e. about 0.173 mm² analyzed each time).

Alloy designation	Ni	Cr	Ta
NCT0	Bal.	/	6.6 ±0.1
NCT1	Bal.	9.9 ±0.2	7.1 ±0.2
NCT2	Bal.	20.6 ±0.3	11.5 ±0.2*
NCT3	Bal.	27.1 ±0.2	10.2 ±0.2*
NCT4	Bal.	40.6 ±0.3	6.2 ±0.3
NCT5	Bal.	51.2 ±0.6	6.2 ±0.2

Carbon content: cannot be controlled; supposed to be well respected